

Language Models and Retrieval Augmented Generation for Automated Structured Data Extraction from Diagnostic Reports: Assessment of Approaches and Parameters

Mohamed Sobhi Jabal ¹; Pranav Warman ²; Jikai Zhang ^{3,4}; Kartikeye Gupta ⁵; Ayush Jain ⁵; Maciej Mazurowski ^{1,2,3}; Walter Wiggins ¹; Kirti Magudia ¹; Evan Calabrese ^{1,5}

Author Affiliations:

1. Department of Radiology, Duke University, Durham, NC, USA
2. Duke University School of Medicine, Durham, NC, USA
3. Department of Electrical and Computer Engineering, Duke University, Durham, NC, USA
4. Duke Center for Artificial Intelligence in Radiology, Duke University, Durham, NC, USA
5. Duke University, Durham, NC, USA
6. Department of Biomedical Engineering, Duke University, Durham, NC, USA

Corresponding Author:

Mohamed Sobhi Jabal
Department of Radiology
Duke University, Durham, NC
mohamedsobhi.jabal@duke.edu

Cover Title: LLM and RAG Configuration for Structured Clinical Data Extraction.

Key Words: Large Language Models; Retrieval Augmented Generation; Radiology; Pathology; Healthcare Reports.

Number of Figures: 6

Number of Tables: 2

Word Count: 3000

Abstract

Purpose: To develop and evaluate an automated system for extracting structured clinical information from unstructured radiology and pathology reports using open-weights large language models (LMs) and retrieval augmented generation (RAG), and to assess the effects of model configuration variables on extraction performance.

Methods and Materials: The study utilized two datasets: 7,294 radiology reports annotated for Brain Tumor Reporting and Data System (BT-RADS) scores and 2,154 pathology reports annotated for isocitrate dehydrogenase (IDH) mutation status. An automated pipeline was developed to benchmark the performance of various LMs and RAG configurations. The impact of model size, quantization, prompting strategies, output formatting, and inference parameters was systematically evaluated.

Results: The best performing models achieved over 98% accuracy in extracting BT-RADS scores from radiology reports and over 90% for IDH mutation status extraction from pathology reports. The top model being medical fine-tuned llama3. Larger, newer, and domain fine-tuned models consistently outperformed older and smaller models. Model quantization had minimal impact on performance. Few-shot prompting significantly improved accuracy. RAG improved performance for complex pathology reports but not for shorter radiology reports.

Conclusions: Open LMs demonstrate significant potential for automated extraction of structured clinical data from unstructured clinical reports with local privacy-preserving application. Careful model selection, prompt engineering, and semi-automated optimization using annotated data are critical for optimal performance. These approaches could be reliable enough for practical use in research workflows, highlighting the potential for human-machine collaboration in healthcare data extraction.

Introduction

Healthcare reports including diagnostic radiology and pathology reports contain vital information necessary for patient care and various clinical and research purposes. Most remain unstructured and challenging to harness. Artificial intelligence (AI) and classical natural language processing (NLP) demonstrated some feasibility for automated data extraction from reports, but considerable challenges included computational cost, variable performance, and ungeneralizable task-specific models. More recently, transformer-based large language models (LMs) have emerged as the preeminent deep learning architecture for a variety of language processing tasks with wide range of potential healthcare applications (1–3). However, using leading commercial LMs requires transfer of data to private companies, which raises considerable privacy concerns for healthcare data and typically requires legal agreements and paid contracts (4–10).

Current development in open-weights LMs offers high performance while mitigating data privacy concerns. Recent studies proposed and demonstrated the potential of LMs and retrieval augmented generation (RAG) for extracting data from clinical documents (11–13). However, one major challenge is the large number of configuration variables to consider including the choice of model, model size, quantization level, embedding models, retrieval strategies, prompting methods, sampling parameters, and output formatting. As each of these factors may affect model performance and computational requirements, comprehensive evaluation of their effects on clinical data extraction tasks is valuable for effective use of these approaches.

This study presents an automated system designed to extract structured clinical information from unstructured healthcare reports using state-of-the-art open-weights LMs and RAG. We examined the LM pipeline configuration influence on data extraction effectiveness using radiology and pathology report datasets from patients with malignant brain tumors. By presenting a structured investigation across various LM architectures and retrieval strategies, this work aims to elucidate recommended strategies for implementing automated clinical data extraction systems from healthcare reports.

Materials and Methods

Dataset and Preprocessing

The study utilized two healthcare report datasets from the same single-institution, retrospectively identified cohort of 1,490 patients undergoing treatment for malignant brain gliomas (adult-type diffuse gliomas, WHO grades 2-4 based on pathologic diagnosis). The radiology dataset consisted of 7,294 radiology reports for brain MRIs with and without contrast performed for brain tumor follow-up, which typically include Brain Tumor Reporting and Data System (BT-RADS) scores at our institution (14,15). Reports were manually annotated for the reported BT-RADS score [0, 1, 1a, 1b, 2, 2a, 2b, 3, 3a, 3b, 3c, 4, or unprovided]. The pathology dataset consisted of 2,154 surgical pathology reports for brain tumor resections including molecular analyses. Reports were manually annotated for the reported isocitrate dehydrogenase (IDH) mutation status [positive - mutant, negative - wildtype, or unprovided]. Non-canonical IDH and IDH-2 mutations were considered “mutant”. Dataset labeling was accomplished using custom, task-specific, rules-based NLP algorithms and subsequently manually reviewed and corrected by a neuroradiologist ([REDACTED for peer review]). The dataset was preprocessed using regex and standard NLP techniques to clean and normalize the text, filtering out newline characters unfollowed by a period and ensuring spaces surrounding newlines after periods, maintaining readability and sentence separation.

Pipeline, Optimization, and Evaluation

We developed an automated pipeline for systematic performance assessment of various LM configuration variables. The benchmarking pipeline was applied on subsets of 500 randomly selected reports from the radiology and pathology datasets. Models were categorized into two groups based on size and computational demand representing high- and low-resource settings: smaller models having $\leq 8\text{B}$ parameters and $\leq 5\text{-bit}$ quantization. The best performing models and configurations were selected for subsequent evaluation on the full dataset. Performance was assessed using accuracy, micro and macro F1, precision, and recall. Independent samples t-test, Welch's t-test assuming unequal variances, and paired t-test were conducted as

applicable. Correlations were examined using Spearman's rank coefficient. All pipeline testing was performed on a workstation equipped with an NVIDIA A6000 48 GB GPU. A generalized adaptation of the report processing pipeline for assessing model configurations is provided at [GitHub/WebApp].

Language Models

The study employed state-of-the-art open-weights LMs to assess their performance in extracting clinical information from the radiology reports (16). The LMs used varied in size, quantization level, training data, release date, medical fine-tuning, and they included Llama3, openbionl- Llama3, Llama2, and Medllama2, Meditron, Mistral, Biomistral, Mixtral, Phi3. Given its recent release, Llama3.1 was applied post-hoc to the entire datasets.

Model Parameters and Quantization

To evaluate the trade-off between model parameter size and performance, we tested a range of small and large parameter-size models. We tested a range of available quantization degrees from 3-bit to 16-bit according to the available levels for each model up to 48 GB VRAM.

Quantization reduces memory and computational needs of language models by using fewer bits to represent parameters. This allows LMs deployment on GPUs with smaller VRAM, at some cost of precision loss.

Prompting Strategies

We evaluated the performance of simple and complex prompting strategies, with and without few-shot prompting. Simple prompting involved a single sentence describing the task, while complex prompting provided detailed instructions on valid responses and output format. Few-shot prompting included examples of correct data extraction and negative examples to handle non-reported data. Models were instructed to format responses as a JSON object schema.

Sampling Parameters

The pipeline systematically evaluated various inference-time sampling parameters' influence on extraction accuracy, specifically: temperature, top-k, and top-p sampling. Temperature, which controls the randomness and indeterministic nature of the model's outputs, was varied across a

range with approximate logarithmic steps [0.0, 0.01, 0.1, 0.5, 0.8]. Top-k sampling, which limits the number of tokens considered and samples from the k most likely next tokens, was investigated at the values: [2, 5, 10, 40]. Top-p sampling controls the cumulative probability cutoff distribution of considered tokens and was investigated at [0.1, 0.5, 0.9].

Output Formatting

To examine effects of enforced standardization of model outputs on performance, we implemented a JSON output formatting from Ollama. This structured output format was compared against prompt instruction to evaluate its extraction accuracy impact.

Retrieval and Embedding Approaches

The pipeline was assessed with and without RAG. The following RAG steps were applied: recursive character text splitting to divide the report into chunks based on sentence separators. Chunk size was set at 70 with 20-character overlap. Embedding model “gte-large” was implemented. Processing was orchestrated using Langchain framework. Text embeddings were stored and indexed in a local vector database (FAISS, Meta AI). Dense retrieval using cosine similarity of vector embeddings was applied to process extracted RAG context chunks, additionally two other optional retrieval approaches were included: hybrid ensemble retrieval combining BM25 with dense retrieval and sequential retrieval using the two methods consecutively. BM25 is a widely used keyword-based search and ranking algorithm that has been essential for many modern search engines (17). A cross-encoder reranker (bge-reranker-v2-m3 from Beijing Academy of Artificial Intelligence) was utilized to sort the retrieved chunks and prioritize the most relevant ones. Keywords relevant to the targeted data point were “follow-up score” and “IDH IDH1 IDH2 IDH1/IDH2 detected positive negative” for radiology and pathology reports, respectively. The retrieved chunk with the highest relevance score was selected, with a relevance score threshold of 0.2, below which RAG was disused.

Postprocessing

Custom postprocessing was applied to the raw language model outputs to enhance consistency and validity. The target datapoint was first extracted, addressing formatting variations such as

delimiters. Artifacts like newline characters, extra whitespace, and inconsistent string quotation marks were removed. Any extraneous text surrounding the desired JSON-formatted output was discarded, and the cleaned response was parsed as a JSON object, retaining only the first valid entry if multiple were present. The extracted information was then validated against the predefined set of valid values for both datasets, with unexpected formats and hallucination edge cases, including null or malformed responses, defaulting to invalid. This postprocessing ensured the final data was clean, consistent, and ready for downstream evaluation.

Results

The performance of 13 language models in 407 different configurations was evaluated on automatically extracting BT-RADS follow-up scores from radiology reports and IDH mutation status from pathology reports. An overview of the pipeline design is provided as Figure 1. Mean radiology report word count was 265 (± 66) with a median of 255 (IQR: 80) words, and the mean pathology report word count was 2504 (± 2563) with a median of 1218 (IQR: 3721) words. The reference standard distribution for BT-RADS follow-up scores in the radiology dataset were: 1: 5 (0.07%), 1a: 204 (2.80%), 1b: 124 (1.70%), 2: 856 (11.74%), 2a: 112 (1.54%), 2b: 10 (0.14%), 3: 88 (1.21%), 3a: 47 (0.64%), 3b: 292 (4.00%), 3c: 386 (5.29%), 4: 373 (5.11%), NR: 4,797 (65.77%). As for IDH mutation reference standard pathology reports, the class distribution was: Positive: 154 (7.15%), Negative: 1559 (72.38%), Not Provided: 441 (20.47%). Sampled examples of the analyzed radiology and pathology reports are provided in Figure 2.

Benchmarking Model Performance

Overall, benchmarking performance varied significantly across different models, configurations, and approaches. On the radiology sampled dataset ($n=500$), accuracy ranged from 62.6% to 98.4% with a mean of 88.4% ($\pm 8.9\%$) and median of 88.8% (IQR: 9.8%). As for the pathology reports, accuracy ranged from 5.2% to 93.6% with a mean of 57.7% ($\pm 27.1\%$) and median of 50.9% (IQR: 45.7%).

Ordered by accuracy, the top performing smaller models were (Acc, M-F1): openbiollm-llama-3 8B Q_4 (99.2%, 98.8), mistral 7B Q_4 (99.0%, 97.9), phi3 4B Q_4 (99.0%, 90.2), llama3 8B

Q_4 (98.4%, 82.4), and biomistral 7B Q_4 (98.0%, 88.0). While the top benchmarked larger models were llama3 70B Q_3 (99.2%, 98.8), mixtral 56B Q_4 (99.2%, 98.8), mistral 7B Q_6 (99.0%, 90.5), openbiollm-llama-3 8B Q_6 (95.2%, 85.5), and phi3 14B Q_5 (93.6%, 82.7).

Model Parameters and Quantization

Larger models demonstrated higher mean accuracy ($86\% \pm 22\%$) compared to smaller ones ($75\% \pm 32\%$) ($t = 3.80$, $p < 0.001$), with medium effect (Cohen's $d = 0.40$). In terms of model parameter size, there was significant positive correlation with accuracy ($r = 0.25$, $p < 0.001$) and macro F1 ($r = 0.18$, $p < 0.001$). Quantization level correlations with performance were statistically non-significant for accuracy ($r = 0.06$, $p = 0.280$) and macro F1 ($r = 0.08$, $p = 0.134$). Illustration of the relationship and correlations between model performance, parameter size, quantization, and recency are demonstrated in Figure 3.

Prompting Strategies

In the radiology dataset, complex prompting consistently improved accuracy across models (32.2% to 98.6% vs. 18.6% to 92.6%). The mean accuracy increase was $12.01\% \pm 11.56\%$ ($t=3.11$, $p=0.01$). Similarly, few-shot prompting improved accuracy in most models. Mean accuracy with few-shot prompting ranged from 21 to 96% vs. 0 to 98.6% without it ($t=3.00$, $p=0.02$), the mean increase being $32.42\% \pm 32.39\%$. When including negative examples in the few-shots method of reports lacking the datapoint of interest, accuracy improved for most models, with accuracy ranging from 34.6-98.0% vs. 16.81-92.61% without negative examples ($t=2.01$, $p=0.08$), and an average accuracy increase of $10.65\% \pm 15.89\%$. Effect of different prompting methods on performance is illustrated in Figure 3.

Sampling Parameters

Regarding temperature, correlations across all metrics were small, ranging from 0.009 to 0.026 ($p=0.78-0.91$), without statistically significant impact on performance. Similarly, top-p and top-k parameters also had minimal correlation of (0.01-0.04, $p=0.76-0.91$) and (0.01-0.03, $p=0.75-0.91$), respectively. Model performance across varying temperature, top-k, top-p is shown in Figure 6.

Output Formatting

In the radiology dataset, enforcing JSON output generally improved accuracy (range with JSON: 12.0%-99.15% vs. without: 20.53%-92.57%, mean change being $+2.92\% \pm 6.78\%$), without statistical significance ($t=1.29$, $p=0.23$). Contrastively, the pathology dataset showed minimal, inconsistent effects from JSON output (range with JSON: 37.3%-69.3% vs. without: 37.3%-68.3%; average change: $-0.44\% \pm 1.54\%$) ($t=-0.64$, $p=0.56$). Effect of forcing JSON output on model accuracy is demonstrated in Figure 5.

Retrieval Augmented Generation

In the radiology sample set, the influence of RAG on accuracy varied widely. The mean accuracy with RAG enabled ranged from 24.0% to 90.8%, compared to 19.73% to 94.35% without RAG. Mean accuracy change was $-7.75\% \pm 31.10\%$ ($t=-0.91$, $p=0.39$). Contrastively in the pathology sample set, RAG consistently improved accuracy across all models. The mean accuracy with RAG ranged from 69.4% to 92.8% vs. 5.2% to 44.8% without RAG, a statistically significant mean increase of $48.08\% \pm 11.18\%$ ($t=7.91$, $p=0.001$). RAG impact on language model performance is shown in Figure 5.

Global Model Performance

The performance of the best model configurations evaluated on the entire radiology ($n=7,294$) and pathology ($n=2,154$) datasets were as follows (Accuracy, Macro F1): On the full radiology dataset, the top 5 results ordered by accuracy were: openbiollm-llama-3 70B Q_4 (98.68%, 90.96%), llama3 70B Q_3 (98.66%, 90.95%), llama3.1 70B Q_4 (98.64%, 90.93%), llama3.1 8B Q_4 (96.74%, 77.80%), phi3 4B Q_4 (94.98%, 87.27%). And for the complete pathology dataset: openbiollm-llama-3 70B Q_4 (90.02%, 85.81%), llama3 70B Q_3 (88.58%, 84.96%), llama3.1 70B Q_4 (85.93%, 75.36%), llama3.1 8B Q_4 (80.22%, 71.97%), phi3 4B Q_4 (76.79%, 65.92%). The overall results are presented in Table 1 and Table 2, respectively.

Discussion

In this study, we developed an automated system for structured clinical data extraction from unstructured radiology and pathology reports using open-weights LMs and RAG approaches.

The top performing models were: openbiollm-llama3:70B, llama3:70B, and llama3.1:70B, achieving over 98% accuracy for radiology BT-RADS score extraction and reaching 90% for pathology IDH mutation status extraction across the entire datasets. These findings demonstrate the technology's significant potential to accurately identify and fetch key clinical information from complex diagnostic reports with minimal human intervention and suggest the models could be reliable enough for practical use in research workflows and automated curation of structured databases from unstructured reports.

Results from our configuration experiments provide potentially helpful insights for designing similar systems for structured data extraction from healthcare reports: First, larger and more recent models consistently and measurably outperformed their counterparts across different settings, conferring an advantage on extraction tasks. A notable exception was Phi:3.8B, a small recent LM performed on par with large models, suggesting model architecture and training can partially compensate for smaller parameter size, which is appealing for local on-device efficient deployment in resource-constrained environments with limited computation capacity. Medically fine-tuned llama3 was the best performing model overall (none was available for llama3.1 at the time of the study). Of note, despite its non-leading performance, llama3.1 features significantly longer context window and improved multilingual capabilities compared to its predecessor. Second, we observed minor performance impact of model quantization across the 3-16-bit range, suggesting VRAM-constrained use-cases should ideally prioritize larger models with low-bit quantization. Third, prompting strategy had significant impact on performance, specifically the use of complex detailed prompts and inclusion of few-shot prompting resulting in notable accuracy increase, underscoring the importance of prompt engineering. Fourth and finally, we found that several inference-time and sampling parameters (temperature, top p, top k) had little or no effect on performance including model.

This study builds upon recent work demonstrating the potential of LMs for healthcare data extraction. Prior studies have shown LMs can extract RADS features with 86-99% accuracy (18) and deduce various categorization from radiology reports with 75% accuracy (19), which

focused primarily on small datasets (30-160 reports) and private commercial LMs regardless of output formatting. Huang et al. assessed LM-based structured data extraction from clinical notes using ChatGPT-3.5 achieving an accuracy of 89% in extracting classifications from 1000 lung cancer pathology reports (20). Glicksberg et al. noted positive observations using GPT-4 for predicting emergency admissions from initial clinical variables with RAG resulting in increased AUC (0.79 to 0.87) (21). Most prior studies focused on commercial LMs, a notable exception was a recent study by Guellec et al., examining open LM (Vicuna) performance in extracting data from 2,398 radiology reports and achieving accuracies > 95%, with unstructured outputs (22).

The study adds to this body of work by exploring recent open LM models and configurations to examine and help identify recommendable parameters across compute capabilities. It further explored the potential impact of RAG and found negative performance effect on relatively short and simple radiology reports and substantial positive performance impact on longer (10-fold) complex pathology reports. The main advantage of RAG lies in increasing signal-to-noise ratio by retrieving only the most relevant sentences, which was especially helpful in reports where the target datapoint (e.g., IDH mutation status) is mentioned multiple times in different contexts throughout the document.

Another key insight was the value of using a semi-automated approach with sampled annotated data for benchmarking and pipeline optimization before full dataset application. This is particularly helpful given the large number of tunable parameters associated with local custom LM systems, given LMs' sensitivity to minor prompt variations, output formatting, and jailbreaking, significantly altering performance (23).

This highlights the crucial interplay between domain expertise and automated AI-systems in healthcare and demonstrates the advantage of partially automated systems in improving accuracy, monitoring, and reliability. At the current phase, we believe human-machine collaboration is the most valid approach for data extraction and research is the most relevant use case. Error rates are expected to drop in the future, which may ultimately enable human

independent implementation and clinical use cases. Recent integration of structured output feature from leading closed LM providers (24) indicates possible future adoption from open frameworks potentially increasing the reliability of valid JSON output generation.

Limitations

Our findings should be considered within the scope and limitations of the study; The radiology and pathology datasets, while relatively large, had fairly homogeneous reporting structure given the single center source. In addition, the chosen target variables had discrete categorical responses, and performance could decrease for more ambiguous datapoints. Finally, while we explored a large configuration space, it was impractical to be exhaustive.

Conclusion

The study highlights the significant potential of open LMs for local automated extraction of structured clinical data from radiology and pathology reports. We found that larger, newer, and domain fine-tuned models had higher performance, that model quantization had minimal effect, that prompt engineering and methods is critical for high performance, and that several inference and sampling parameters had little to no effect. RAG significantly improved performance in complex and lengthy pathology reports. Depending on report complexity, top-performing model configurations achieved 90% to 98% accuracy in structured extracting of clinical datapoints underscoring the approach reliability for practical use in research workflows. Semi-automated systems with human oversight and iterative optimization using partially annotated data proved important when developing LM systems.

References

1. Clusmann J, Kolbinger FR, Muti HS, et al. The future landscape of large language models in medicine. *Commun Med (Lond)*. Springer Science and Business Media LLC; 2023;3(1):1–8.
2. Meng X, Yan X, Zhang K, et al. The application of large language models in medicine: A scoping review. *iScience*. Elsevier BV; 2024;27(5):109713.
3. Nerella S, Bandyopadhyay S, Zhang J, et al. Transformers and large language models in healthcare: A review. *Artif Intell Med*. Elsevier BV; 2024;154(102900):102900.
4. Chen Y, Esmailzadeh P. Generative AI in medical practice: In-depth exploration of privacy and security challenges. *J Med Internet Res*. JMIR Publications Inc.; 2024;26:e53008.
5. Ong JCL, Chang SY-H, William W, et al. Medical ethics of large language models in medicine. *NEJM AI*. Massachusetts Medical Society; 2024;1(7). doi: 10.1056/aira2400038.
6. Rahman MA. A survey on security and privacy of multimodal LLMs - connected healthcare perspective. *2023 IEEE Globecom Workshops (GC Wkshps)*. IEEE; 2023. p. 1807–1812.
7. Denecke K, May R, LLMHealthGroup, Rivera Romero O. Potential of large language models in health care: Delphi study. *J Med Internet Res*. JMIR Publications Inc.; 2024;26:e52399.
8. Cohen IG. What should ChatGPT mean for bioethics? *Am J Bioeth*. Informa UK Limited; 2023;23(10):8–16.
9. Ullah E, Parwani A, Baig MM, Singh R. Challenges and barriers of using large language models (LLM) such as ChatGPT for diagnostic medicine with a focus on digital pathology – a recent scoping review. *Diagn Pathol*. Springer Science and Business Media LLC; 2024;19(1). doi: 10.1186/s13000-024-01464-7.

10. Meskó B, Topol EJ. The imperative for regulatory oversight of large language models (or generative AI) in healthcare. *NPJ Digit Med*. Springer Science and Business Media LLC; 2023;6(1):1–6.
11. Alkhalaf M, Yu P, Yin M, Deng C. Applying generative AI with retrieval augmented generation to summarize and extract key clinical information from electronic health records. *J Biomed Inform*. Elsevier BV; 2024;156(104662):104662.
12. Kresevic S, Giuffrè M, Ajcevic M, Accardo A, Crocè LS, Shung DL. Optimization of hepatological clinical guidelines interpretation by large language models: a retrieval augmented generation-based framework. *NPJ Digit Med*. Springer Science and Business Media LLC; 2024;7(1). doi: 10.1038/s41746-024-01091-y.
13. Zakka C, Shad R, Chaurasia A, et al. Almanac - retrieval-augmented language models for clinical medicine. *NEJM AI*. Massachusetts Medical Society; 2024;1(2). doi: 10.1056/aioa2300068.
14. Zhang JY, Weinberg BD, Hu R, et al. Quantitative improvement in brain tumor MRI through structured reporting (BT-RADS). *Acad Radiol*. Elsevier BV; 2020;27(6):780–784.
15. Gore A, Hoch MJ, Shu H-KG, Olson JJ, Voloschin AD, Weinberg BD. Institutional implementation of a structured reporting system: Our experience with the Brain Tumor Reporting and Data System. *Acad Radiol*. Elsevier BV; 2019;26(7):974–980.
16. HuggingFace Open LLM Leaderboard. . https://huggingface.co/spaces/open-llm-leaderboard/open_llm_leaderboard. Accessed April 2024.
17. Robertson S, Zaragoza H. The probabilistic relevance framework: BM25 and beyond. *Found Trends® Inf Retr*. Now Publishers; 2009;3(4):333–389.

18. Gu K, Lee JH, Shin J, et al. Using GPT-4 for LI-RADS feature extraction and categorization with multilingual free-text reports. *Liver Int. Wiley*; 2024;44(7):1578–1587.
19. Wu Q, Wu Q, Li H, et al. Evaluating large language models for automated Reporting and Data Systems categorization: Cross-sectional study. *JMIR Med Inform. JMIR Publications Inc.*; 2024;12:e55799.
20. Huang J, Yang DM, Rong R, et al. A critical assessment of using ChatGPT for extracting structured data from clinical notes. *NPJ Digit Med. Springer Science and Business Media LLC*; 2024;7(1). doi: 10.1038/s41746-024-01079-8.
21. Glicksberg BS, Timsina P, Patel D, et al. Evaluating the accuracy of a state-of-the-art large language model for prediction of admissions from the emergency room. *J Am Med Inform Assoc. Oxford University Press (OUP)*; 2024; doi: 10.1093/jamia/ocae103.
22. Le Guellec B, Lefèvre A, Geay C, et al. Performance of an open-source large language model in extracting information from free-text radiology reports. *Radiol Artif Intell. Radiological Society of North America (RSNA)*; 2024;6(4). doi: 10.1148/ryai.230364.
23. Fan B, García-García AM. Quenched dynamics and pattern formation in clean and disordered Bogoliubov-de Gennes superconductors. *arXiv [cond-mat.supr-con]*. 2023.
<http://arxiv.org/abs/2401.00372>. Accessed August 16, 2024.
24. OpenAI - Introducing Structured Outputs in the API. . <https://openai.com/index/introducing-structured-outputs-in-the-api/>. Accessed August 2024.

Tables

Table 1. Language model performance on the entire radiology report dataset.

Language Model	Parameters	Quantization	Accuracy	Macro Precision	Micro Precision	Macro Recall	Micro Recall	Macro F1	Micro F1
Openbiollm-llama3	70	4	98.68%	90.48	98.68	91.45	98.68	90.96	98.68
Llama3	70	3	98.66%	90.48	98.66	91.44	98.66	90.95	98.66
Llama3.1	70	4	98.64%	90.52	98.64	91.35	98.64	90.93	98.64
Llama3.1	8	4	96.74%	75.92	96.74	84.73	96.74	77.8	96.74
Llama3	8	4	96.22%	75.55	96.22	84.77	96.22	77.86	96.22
Phi3	4	4	94.98%	84.78	94.98	90.86	94.98	87.27	94.98
Biomistral	7	4	86.5%	66.51	86.5	84.06	86.5	70.32	86.5
Mixtral	56	8	45.19%	90.27	45.19	67.01	45.19	74.43	45.19

Table 2. Language model performance on the entire pathology report dataset.

Language Model	Parameters	Quantization	Accuracy	Macro Precision	Micro Precision	Macro Recall	Micro Recall	Macro F1	Micro F1
Openbiollm-llama-3	70	4	90.02%	82.47	90.02	90.38	90.02	85.81	90.02
Llama3	70	3	88.58%	82.08	88.58	89.44	88.58	84.96	88.58
Llama3.1	70	4	85.93%	77.19	85.93	77.25	85.93	75.36	85.93
Mixtral	56	8	84.35%	63.13	84.35	63.34	84.35	62.69	84.35
Llama3.1	8	4	80.22%	72.58	80.22	76.33	80.22	71.97	80.22
Biomistral	7	4	77.48%	49.14	77.48	51.71	77.48	45.93	77.48
Phi3	4	4	76.79%	62.76	76.79	77.1	76.79	65.92	76.79
Llama3	8	4	42.25%	66.17	42.25	68.25	42.25	52.74	42.25

Figures

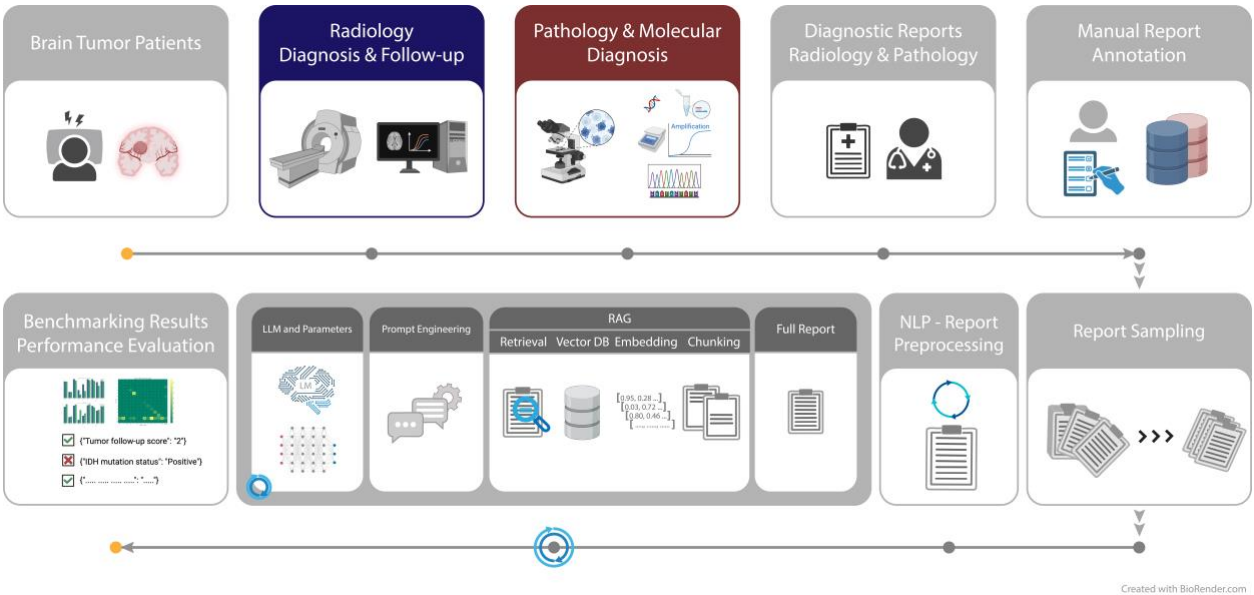


Figure 1. Overview of the study workflow demonstrating the different steps from diagnosis to automated structured data extraction of relevant follow-up and clinical information from diagnostic radiology and pathology reports.

Sampled Radiology Report	Sampled Pathology Report
<p>Sampled full report: 364 words:</p> <p>Procedure: MRI BRAIN WITHOUT AND WITH CONTRAST</p> <p>INDICATION: Neoplasm: head, CNS, recurrence, suspected/known, Neoplasm: head, CNS, rx monitor or follow up, Neoplasm: head, CNS, staging, Neoplasm: head, CNS, suspected, C71.1 Malignant neoplasm of frontal lobe (CMS-HCC)</p> <p>COMPARISON: *****</p> <p>TECHNIQUE/PROTOCOL: Standard adult brain protocol.</p> <p>CONTRAST: 17ml, MultiHance IV. This MRI was performed before and after IV administration of contrast material. IV contrast was administered to improve disease detection and further define anatomy.</p> <p>* GFR: ***** measured</p> <p>* Complications: No immediate patient complications or events noted.</p> <p>FINDINGS:</p> <p>Postoperative changes of right frontal craniotomy with subjacent resection cavity redemonstrated. There is increased T2/FLAIR hyperintense signal adjacent the resection cavity extending into the left frontal lobe, right temporal lobe, and right frontal lobe. Redemonstration of thick enhancement surrounding the posterior/lateral margin of the resection cavity. Redemonstration of numerous foci of contrast enhancement throughout the right frontal lobe, left frontal lobe and right temporal lobe. Increased size of enhancing lesions, particularly within the left frontal lobe. For example (series 9 image 21) a an index lesion measures approximately 1.2 x 2.2 cm compared to prior 1.7 x 1.0 cm. There is increased enhancement along the left temporal horn concerning for new ependymal spread.</p> <p>Additional Parenchyma Findings: No evidence of acute infarct or hemorrhage. No new mass effect.</p> <p>Basal Cisterns/Ventricles/Sylvian Fissures: Stable configuration of the cisterns and ventricles. Normal sulcation for age.</p> <p>Extra-Axial Spaces: No extra-axial fluid collection.</p> <p>Intracranial Flow-Voids: Normal</p> <p>Midline Structures and Posterior Fossa: The pituitary, mammillary bodies, tectal plate and posterior fossa appear normal. Redemonstration of at least moderate central canal stenosis at C3-C4. Redemonstration of abnormal enhancement of the genu of the corpus callosum.</p> <p>Orbits and Soft Tissues: Bilateral cataract surgery.</p> <p>Paranasal and Mastoid Sinuses: Normal</p> <p>IMPRESSION:</p> <p>Increased size of multiple foci of enhancement, particularly within the left frontal lobe as well as increased T2/FLAIR signal involving the bilateral frontal lobes and left temporal lobe. Brain tumor follow-up score 4: Imaging worsening, highly suspicious for tumor progression</p> <p>Electronically Reviewed by: ***** MD, ***** Radiology</p> <p>Electronically Reviewed on: *****</p> <p>I have reviewed the images and concur with the above findings.</p> <p>Electronically Signed by: ***** MD, ***** Radiology</p> <p>Electronically Signed on: *****</p>	<p>Sampled 665 words (from full report of 3240 words):</p> <p>... 775 words preceding.</p> <p>Section:Sample Type</p> <p>UNSTAINED SLIDES, ***** "A3" FOR IDH1 TARGETED MUTATION ANALYSIS WITH REFLEX TO IDH2</p> <p>Section:Methodology</p> <p>This assay uses PCR amplification followed by Sanger DNA sequencing to detect point mutations in exon 4 of the IDH1 gene, with reflex testing to detect point mutations in exon 4 of the IDH2 gene for all IDH1 negative cases. An H&E stained slide for each case is first evaluated to identify the regions of greatest tumor content. These regions are then macro-dissected from adjacent unstained formalin-fixed paraffin-embedded sections and used to prepare genomic DNA. The protein coding and flanking intronic sequences of IDH1 exon 4 (containing codon 132), and, if reflex testing is performed, IDH2 exon 4 (containing codon 172) are amplified from this purified genomic DNA by PCR.</p> <p>... 191 words ...</p> <p>Sequences are compared to the reference DNA sequence for the IDH1 and IDH2 genes. (GenBank Accession IDH1: NM_005896.2; IDH2: NM_002168.2)</p> <p>... 68 words ...</p> <p>Section:Objective Findings</p> <p>IDH1: No mutation detected. Complete coverage of IDH1 exon 4 (amino acids 69-138) was obtained using forward and reverse sequencing primers. These sequences were compared to the reference DNA sequence (GenBank Accession: NM_005896.2).</p> <p>This sample was also tested for IDH2 mutations with the following result:</p> <p>IDH2: No mutation detected. Complete coverage of IDH2 exon 4 (amino acids 126-178) was obtained using forward and reverse sequencing primers. These sequences were compared to the reference DNA sequence (GenBank Accession: NM_002168.2).</p> <p>Section:INTERPRETATION</p> <p>UNSTAINED SLIDES, ***** "A3" (IDH1 TARGETED MUTATION ANALYSIS WITH REFLEX TO IDH2):</p> <p>NEGATIVE.</p> <p>IDH1 AND IDH2 MUTATIONS NOT DETECTED. SEE COMMENT AND OBJECTIVE FINDINGS.</p> <p>COMMENT: Isocitrate dehydrogenase 1 and 2 (IDH1 and IDH2) are NADP+ dependent enzymes that catalyze the conversion of isocitrate to alpha-ketoglutarate and are key components in the mitochondrial citric acid cycle. Acquired point mutations in primary CNS neoplasms have been described in codon 132 of IDH1 (predominantly Arg132His, but also Arg132Cys, Arg132Ser, Arg132Leu and Arg132Gly) and the analogous amino acid in IDH2 (Arg172Gly, Arg172Lys and Arg172Met). A high percentage of WHO grade II and grade III astrocytic and oligodendroglial neoplasms contain IDH1 or IDH2 mutations, including diffuse astrocytomas (II), oligodendrogliomas (II), anaplastic astrocytomas and oligodendrogliomas (III) and anaplastic oligoastrocytomas (III). IDH1 and IDH2 mutations are also common in secondary glioblastomas (IV) but are rarely found in primary adult or pediatric glioblastomas (IV). In patients with glioblastomas or anaplastic astrocytomas, the presence of an acquired IDH1 or IDH2 mutation is associated with longer overall survival. Multiple factors contribute to prognosis in patients with primary CNS neoplasms.</p> <p>Thus, this assay is intended for use as an aid in developing patient-specific prognostic predictions but is not a substitute for a complete pathologic and clinical evaluation, or physician's judgment and clinical experience. The sensitivity and specificity of DNA sequencing is high for the detection of nucleotide base changes, small deletions, and insertions in the regions analyzed. This assay may not detect an acquired mutation that is present below the 15% detection limit (i.e., mutant cell population of <30%). Only amino acids 69-138 of the IDH1 gene and amino acids 126-178 of the IDH2 gene were examined. Changes outside of this region will not be detected. The presence of a mutant population containing a large deletion, duplication, insertion, aberrant splicing, or sequence alteration adversely affecting primer binding may not be identified using these methods. Mutations or polymorphisms in the DNA oligonucleotide primer binding regions, poor DNA quality, insufficient DNA quantity or the presence of PCR inhibitors can result in uninterpretable or (rarely) inaccurate results. For additional information or for help interpreting the results of this test, clinicians should contact the DUHS Clinical Molecular Diagnostics Laboratory. Patients should contact their healthcare provider with any questions related to this report.</p> <p>References:</p> <p>Babus J, et al. Analysis of the IDH1 codon 132 mutation in brain tumors. Acta Neuropathol. 2008;116:597-602.</p> <p>Yan H, et al. IDH1 and IDH2 mutations in gliomas. N Engl J Med. 2009;360(8):765-73.</p> <p>Section:Molecular Diagnostics Director</p> <p>*****</p> <p>... 241 words ...</p> <p>Section:Diagnosis</p> <p>A. "BRAIN TISSUE" (RESECTION):</p> <p>GLIOBLASTOMA (WHO GRADE IV)</p> <p>Section:Addendum 1</p> <p>Testing was performed on sample *****.</p> <p>Please see MOLECULAR DIAGNOSTICS Report ***** for complete report.</p> <p>IDH1 WITH REFLEX TO IDH2 MUTATION INTERPRETATION:</p> <p>NEGATIVE</p> <p>IDH1 AND IDH2 MUTATION NOT DETECTED</p> <p>Please see MOLECULAR DIAGNOSTICS Report ***** for complete report.</p> <p>TERT MUTATION INTERPRETATION:</p> <p>POSITIVE</p> <p>TERT PROMOTER MUTATION DETECTED</p> <p>COMMENT:</p> <p>THIS PATTERN OF IDH1 AND IDH2 INTACT WITH MUTATED PROMOTER REGION OF TERT IS CONSISTENT WITH A PRIMARY GLIOBLASTOMA GENOTYPE.</p> <p>...1,300 words succeeding.</p>

Figure 2. Sampled examples of processed radiology and pathology reports with highlighted datapoints of interest in yellow and retrieved context using RAG in green.

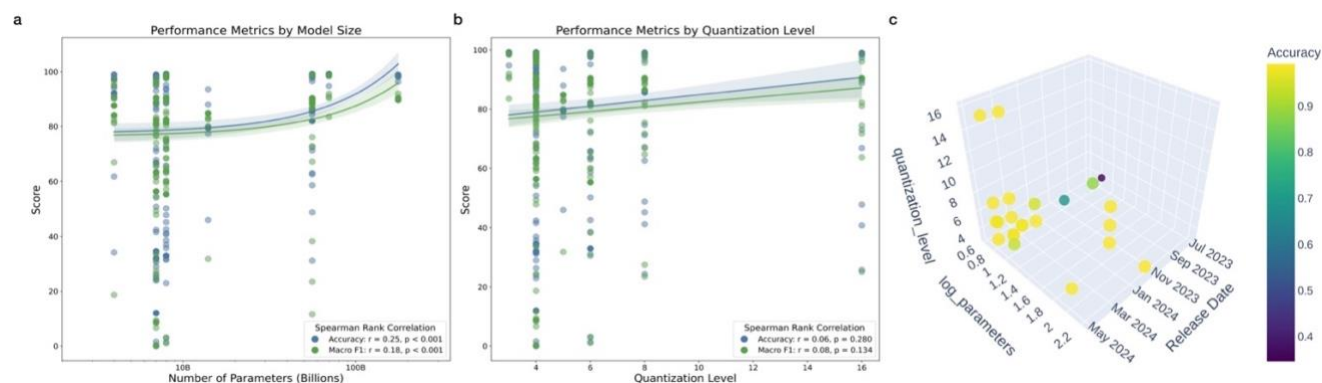


Figure 3. Correlation plots showing the relationships between model performance metrics (accuracy and macro F1 score) versus logarithm of model parameter size and model quantization level (a, b). Size and release date distribution of deployed language models with correlated performance for structured clinical data extraction from radiology reports (c).

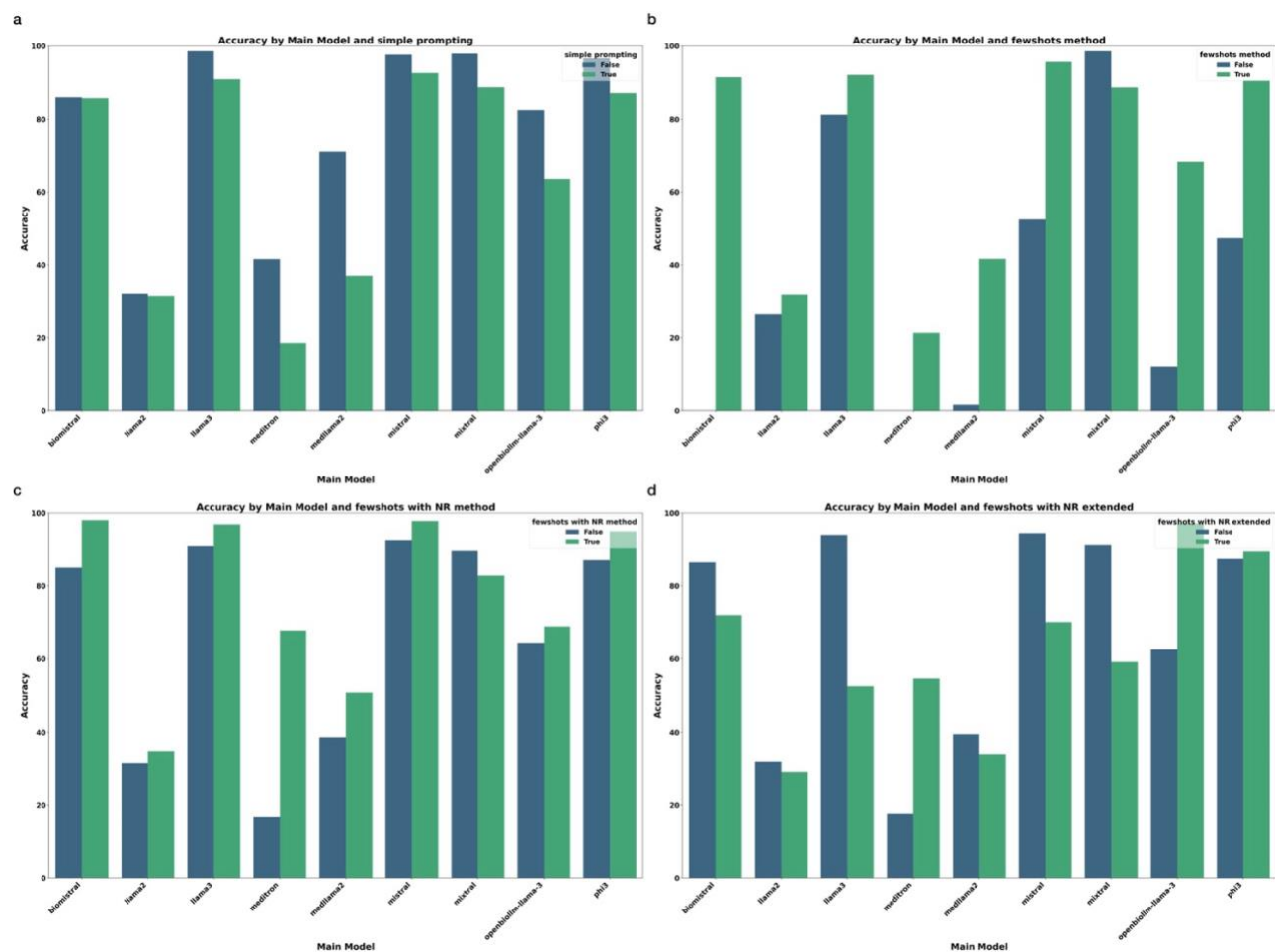


Figure 4. Language model performance comparing simple and complex detailed prompting approaches (a) and fewshots methods with positive (b) and negative non-reported (NR) examples (c, d) for structured clinical data extraction from radiology reports.

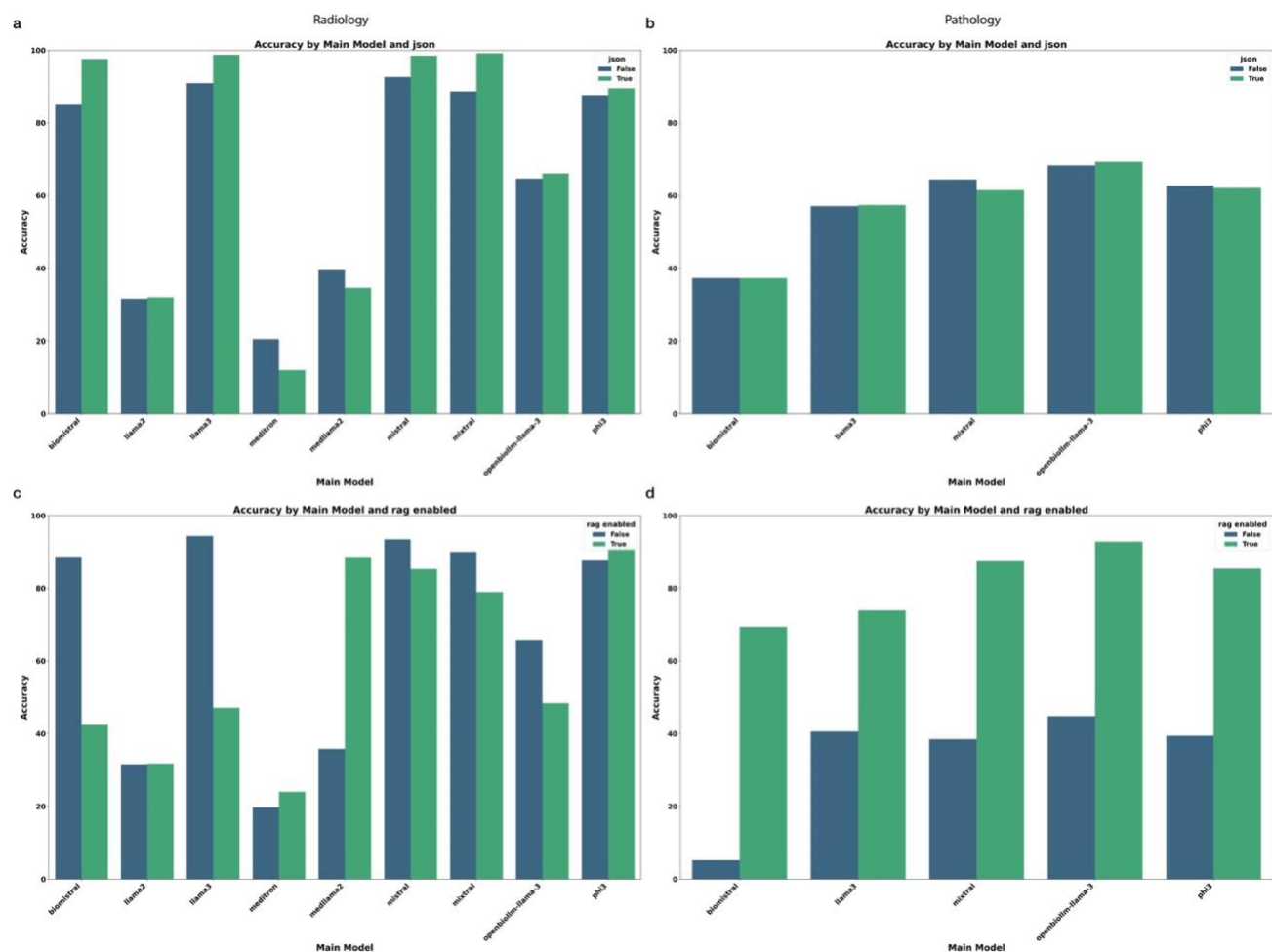


Figure 5. Language model performance evaluating the effect of forcing JSON outputs and adopting RAG for structured clinical data extraction from radiology (a, c) and pathology (b, d) reports.

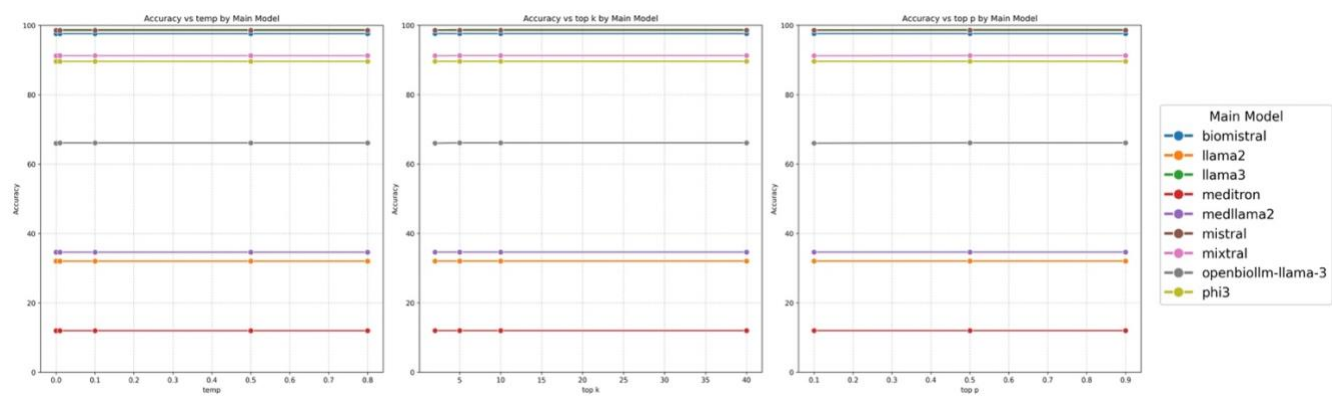


Figure 6. Language model performance across varying inference-time parameters, temperature, top p, and top k for structured clinical data extraction from radiology reports.